Applied Catalysis B: Environmental 284 (2021) 119722

Contents lists available at ScienceDirect

Applied Catalysis B: Environmental

journal homepage: www.elsevier.com/locate/apcatb

Atomically Dispersed Dopants for Stabilizing Ceria Surface Area

Ryan Alcala [a], Andrew DeLaRiva [a], Eric J. Peterson [a], Angelica Benavidez [a], Carlos E. Garcia-Vargas [b], Dong Jiang [b], Xavier Isidro Pereira-Hernández [b], Hidde H. Brongersma [c], Rik ter Veen [d], Jan Staněk [e], Jeffrey T. Miller [f], Yong Wang [b,g], Abhaya Datye [a,*]

[a] Department of Chemical and Biological Engineering and Center for Microengineered Materials, University of New Mexico, Albuquerque, New Mexico 87131, USA
[b] The Gene and Linda Voiland School of Chemical Engineering and Bioengineering, Washington State University, Pullman, WA 99164, USA
[c] ION-TOF GmbH, Heisenbergstr. 15, 48149 Münster, Germany
[d] Tascon GmbH, Mendelstr. 17, 48149 Münster, Germany
[e] Institute of Physical Engineering, Faculty of Mechanical Engineering, Brno University of Technology, Technická 2, Brno, Czech Republic
[f] Davidson School of Chemical Engineering, Purdue University, 480 Stadium Mall Drive, West Lafayette, IN 47907-2100, USA
[g] Institute for Integrated Catalysis, Pacific Northwest National Laboratory, Richland, WA 99354, USA

ARTICLE INFO

Keywords:
Thermal stability
sintering
cerium oxide
single atom catalyst
surface mobility

ABSTRACT

Ceria is known to be a very good catalyst as well as a support for oxygen transfer (oxidation) as well as for hydrogen transfer (hydrogenation and dehydrogenation) reactions. Many of these reactions occur at high temperatures where ceria is known to sinter, leading to loss of surface area. The thermal stability of ceria can be improved by the addition of dopants, but the location of the dopant atoms and the mechanisms by which ceria stabilization occurs are poorly understood. We show here that dopants located on the surface of ceria are remarkably effective at stabilizing ceria surface area. Keeping metal loading constant at 0.88 mol%, we found that surface area of the ceria aged at 800 °C in air for 5 h ranged from 45 m^2/g to 2 m^2/g. Strongly bound dopants in atomically dispersed form help to pin surface sites and lower the mobility of ceria.

1. Introduction

Ceria has been shown to be a beneficial oxide support for multiple catalytic reactions such as the water-gas shift reaction, CO oxidation, dry reforming of methane, oxidation of hydrocarbons (such as methane), among others [1,2]. The reason is its ability to change oxidation states (Ce^{4+}/Ce^{3+}), which may provide facile transfer of oxygen to the active site [3]. The hydrogenation activity of ceria is a more recent finding, related to the formation of hydrides [4,5]. The ceria support, however, loses surface area (sinters) when exposed to high temperatures (>600 °C). The most common method to improve its surface area stability is to dope the bulk ceria with zirconia (Zr) forming solid solutions, which are commonly used in automotive exhaust catalysts [6–8]. Zirconia is unique since it can be incorporated in the fluorite ceria lattice at high concentrations, due to its favorable charge and ionic size, without leading to phase segregation [6–8]. However, the number of dopants that can be similarly incorporated into the ceria lattice is limited [1]. Other approaches for achieving high ceria surface areas involve the deposition of ceria on a thermally stable support via atomic layer deposition (ALD) [9]. An alternative approach that we have used here involves the deposition of dopants on the surface of the ceria.

For a dopant to be effective at stabilizing the surface area, it must be strongly bound to surface sites helping to lower surface mobility of the ceria. It is known that lanthanum oxide helps to preserve alumina surface area through strong binding to the surface [10]. It would be of interest to determine if a similar surface stabilization could be achieved for ceria surfaces. The recent work of Jones et al. [11] suggests a simple approach for screening surface dopants to determine whether they bind strongly to the ceria surface. Impregnation of the ceria with a platinum precursor, followed by calcination in air at 800 °C, leads to the formation of atomically dispersed Pt species on the ceria surface. Concurrent with the formation of single atom Pt species was the stabilization of the ceria surface area. Kunwar et al. showed that the Pt was located on CeO_2 (111) step edges in the form of Pt^{2+} bound to four oxygen atoms [12]. The covalent bonding of Pt^{2+} to the ceria surface was responsible for the enhanced thermal stability. Vapor phase transport was considered to be

* Corresponding author.
E-mail address: datye@unm.edu (A. Datye).

https://doi.org/10.1016/j.apcatb.2020.119722
Received 1 July 2020; Received in revised form 29 October 2020; Accepted 30 October 2020
Available online 21 November 2020

responsible distributing the Pt effectively over the ceria surface, allowing it to attach to defect sites [12]. It is unclear whether a volatile oxide is essential to achieve ceria surface area stabilization. For instance Wan and Dettling deposited aluminum precursors on ceria and found that a BET surface area of 21.5 m^2/g was obtained after aging the sample at 750 °C for 70 hours in air [13]. No volatile precursor was implicated in that work. Therefore, in this work, we explore whether a similar stabilization of ceria surface area can be achieved with elements other than Pt or Al.

To explore a broader range of surface dopants, we turn to the work of Figueroba et al. [14] who performed density functional theory calculations to calculate the binding energy for Fe, Ru, Os, Co, Rh, Ir, Ni, Pd, Cu, Ag, and Au on ceria. They suggested that each of these elements can form single atom species in preference to forming larger nanoparticles. In addition, Pt, Pd, Ni, Fe, Co, and Os were found to exhibit strongly adsorption complexes with the ceria (100) facet with potential for the design of single atom catalysts [14]. Here we explore whether these predictions also suggest dopants for stabilization of ceria surface area.

2. Experimental Methods

2.1. Surface Doping

Polyhedral ceria (PHC) was prepared via the decomposition of cerium (III) nitrate hexahydrate 99.9% obtained from Sigma Aldrich. The nitrate was placed into a crucible and decomposed in a box furnace at 350 °C for 4 hours with a 1 °C per minute ramp rate. The resulting solid was then ground to a powder and was used as the cerium oxide support for the multiple transition metals used in this study.

Transition metals were deposited onto the surface of the PHC support via incipient wetness impregnation (IWI). One gram of polyhedral ceria was placed into a crucible and the dissolved transition metal nitrate hydrate was added drop wise until saturation. The powder was then placed in a drying oven at 110 °C until completely dry. This process was repeated until the desired 0.88 mol% was achieved for all tested metals. 0.88 mol% is the molar equivalent of 1 wt% Pt/CeO_2 and was used to allow for a comparison while maintaining an identical ratio of dopant per cerium atom ($M_{0.88}Ce_{99.12}O_y$). The dried powder was then distributed evenly in a crucible and calcined in a tube furnace at 350 °C for 2 hours with a 5 °C/min ramp rate. After this treatment the samples were labeled as-prepared (AP). The samples were then divided into aliquots to be calcined at 800 °C for 5 hours with a 5 °C/min ramp rate; these samples will be referred to as atom trapped (AT). A schematic of the resulting evolution of ceria is shown below in Fig. 1.

2.2. Physical Characterization

The samples were characterized using Brunauer-Emmett-Teller (BET) surface area analysis, X-ray diffraction (XRD), transmission electron microscopy (TEM), energy dispersive spectroscopy (EDS), and low energy ion scattering (LEIS). BET analysis of all samples was performed using a Micromeritics Gemini 2360 Surface Area Analyzer, using liquid nitrogen coolant, after a 24 -h degassing period at 120 °C under flowing nitrogen gas. XRD analysis was conducted using a Rigaku SmartLab diffractometer with a D/TeX detector and copper Kα radiation. A 0.02° step size was used with a scan rate of 6.2° min^{-1}. TEM analysis was performed using a JEOL JEM 2010 F field emission microscope in high angle annular dark field (HAADF) imaging and EDS mapping modes. Some of the images were obtained using a JEOL NeoARM microscope equipped with spherical aberration correction to allow atomic resolution imaging.

2.3. X-ray Diffraction

X-ray diffraction data was collected using a Rigaku SmartLab powder x-ray diffractometer, equipped with a Cu-target X-ray source (40 kV, 40 mA), a D/teX Ultra 1-dimensional position sensitive detector, and a Ni-foil filter for reduction of the Cu-Kβ component of the diffracted radiation. Data was collected at 6 degrees/minute from 3-150 degrees two theta (0.02-degree step). Lattice parameters were obtained via Rietveld refinement using the MDI Jade software package. Lattice parameters, crystallite size, and micro strain values were refined, as well as sample height error.

2.4. Catalytic Reactivity

CO oxidation was chosen as a probe reaction. 20 mg of catalyst was placed in a quartz tube and a flow rate of 1.5 ml/min of CO and 1.0 ml/min of O_2 along with 75 ml/min of He was used as the reaction mixture. The catalyst was calcined in-situ at 500 °C in 20% oxygen to clean the surface before reaction. No reduction was performed. Three runs were performed by flowing the reaction mixture starting from 25 °C and heating to 300 °C at a ramp rate of 2 °C/min. No intermediate treatment was performed. The third run was reported as representing the reactivity of the stable catalyst, but the variation from run to run was negligible.

2.5. Infrared Spectroscopy

Diffuse Reflectance Infrared Fourier Transform Spectroscopy

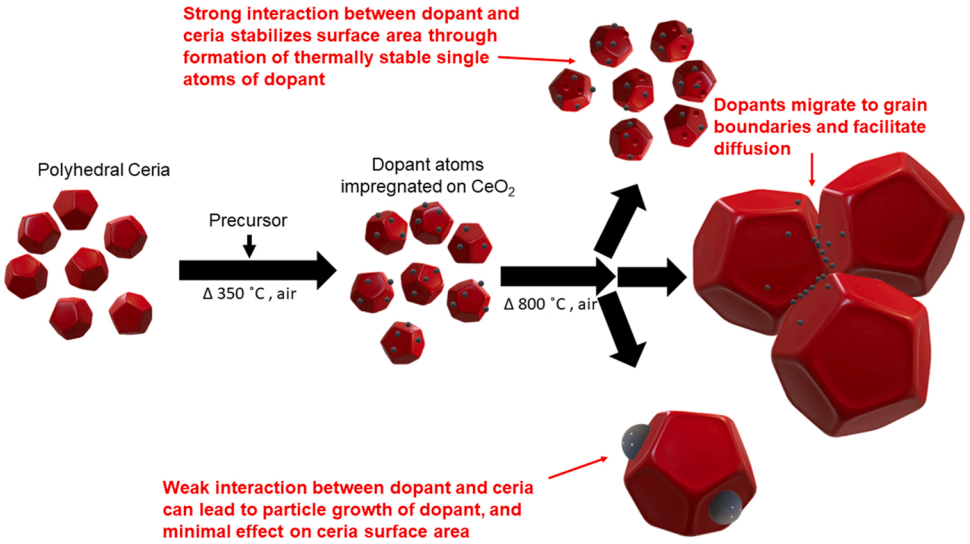

Fig. 1. Schematic representation of the role of dopants on ceria surface area. The transition metal is deposited by impregnation, calcined at 350 °C in air, and then aged at 800 °C in air for 5 hours. If the dopant binds strongly to the ceria, it can remain atomically dispersed and helps preserve ceria surface area by pinning sites responsible for ceria mobility. If the dopant binds strongly but leads to grain boundary diffusion, it could enhance sintering and lead to loss of surface area. Alternatively, the dopant may interact weakly and have no effect on ceria surface area, ending up forming a separate phase.

(DRIFTS) was performed to study the adsorbed CO during CO oxidation. This measurement allowed a study of the surface species for Pt, Pd and Cu. The 800 °C air-aged, air-exposed catalyst was loaded into the DRIFTS cell and temperature was increased to 300 °C in He. Once at 300 °C, a pretreatment with 10% O_2 was performed for 30 minutes. The gas was switched to He, the catalyst cooled to the reaction temperature, and CO oxidation was performed. The gas flow rates for CO oxidation were as follows: CO 1.5 mL/min, O_2 1 mL/min, and He 75 mL/min. The infrared spectrometer used was a Tensor 27 from Bruker, coupled with a Praying Mantis Diffuse Reflection Accessory from Harrick. The MS used was a ThermoStar GSD 320 T Quadropole Mass Spectrometer (QMS) from Pfeiffer Vacuum, using a Secondary Electron Multiplier (SEM). DRIFTS was performed using a Harrick cell which allowed treatment of samples in situ.

2.6. Low Energy Ion Scattering (LEIS)

LEIS analysis was performed on an IONTOF Qtac100 instrument, which is a dedicated LEIS instrument, equipped with a double toroidal analyzer for the energy analysis of the backscattered ions. The solid angle of acceptance was full 360° azimuth, while the scattering angle is fixed at 145°. This gives, in combination with parallel energy detection, a high sensitivity while maintaining the mass resolution. He^+ as well as Ne^+ with ion energy 3 and 5 keV and current 5 and 2 nA, respectively, were used to analyze the surface concentration of Rh atoms in the Rh/CeO_2 (surface doped). The area scanned per sample by these two ions was 2×2 mm^2 and the ion fluence (number of incident particles / area) given to the samples was 1.4×10^{14} ions/cm^2 and 2.8×10^{13} ions/cm^2 respectively. For the 5 keV $^{20}Ne^+$ spectra of the sample, three positions were analyzed, and the spectra were averaged. The spectra for the Rh reference were analyzed within a 1.5×1.5 mm^2 sputter crater over an area of 1×1 mm^2. The analysis time was adjusted such that the surface damage was the same as for the other spectra. Assuming a sputter coefficient of 0.1 for He and 1 for Ne, this will lead to a removal of 1% and 2% of surface atoms by the end of the analysis. Damage would also include the formation of structural changes, defects, etc.

2.7. X-ray Photoelectron Spectroscopy

XPS measurements were performed on a Kratos Ultra DLD spectrometer using amonochromatic Al Kα source operating at 150 W (1486.6 eV). The operating pressure was 1×10^{-8} Torr. Survey scans were acquired at a pass energy of 160 eV with a step size of 1 eV. High-resolution spectra were acquired at a pass energy of 20 eV and a step size of 0.1 eV. Spectra were energy-corrected according to the u''' component of the Ce 3d core line with a characteristic binding energy of 916.7 eV. Atomic ratios were estimated by using the standard procedure of subtracting a Shirley background and using relative sensitivity factors to normalize raw peak areas. The Ce 3d region was fitted according to previous models [15]. XPS data was processed using CasaXPS software.

3. Results

We use the loss of BET surface area after heating to 800 °C in air to study the role of dopants and their interaction with the ceria. In previous work we demonstrated that Pt present on the surface of ceria helps to preserve ceria surface area [11,12]. In this work, we use the Pt/ceria sample as a standard with which to compare the ability of other surface dopants to stabilize ceria surface area. We found that Rh, Zr, Pd, Ga, Al, Mn, Ba, Pr, and Cu, help to preserve ceria surface area after heating to 800 °C in air for 5 hours, as shown in Fig. 2. La and Ag are not very effective, while Fe and Co lead to lower surface areas than undoped CeO_2. The average ceria particle size by XRD agrees well with the measured BET surface area (Table S1). The higher surface area samples have an average crystallite size (via XRD) of ~20 nm while the sintered ceria grows to ~ 80 nm in size. XRD of the Ag, Fe and Co doped samples shows very sharp peaks, suggesting significant sintering of the ceria (Figure S1). STEM images (Figure S2-S3) show particle sizes as small as 2 nm, but they are agglomerated, which is consistent with the observed surface area. Fig. 3 shows XRD patterns of the samples that retain a higher surface area than Pt, with the as-prepared ceria shown for comparison. There are no other reflections than those from fluorite ceria. This suggests that the dopant atoms are well dispersed to at least to the size of (<2 nm) which is the detection limit for XRD under our

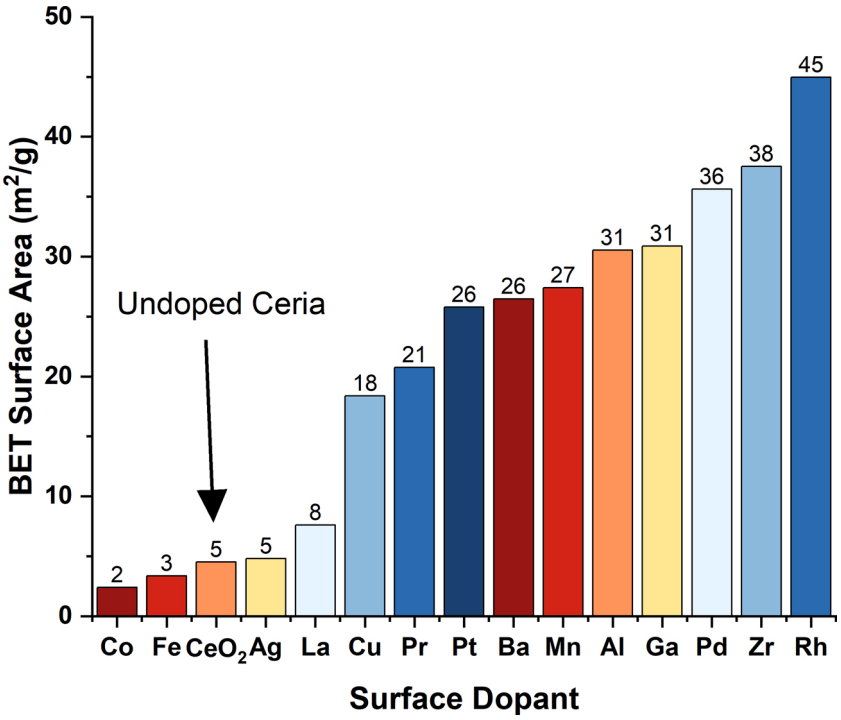

Fig. 2. Measured BET surface area of surface doped ceria after aging in 50 SCCM of flowing air at 800 °C for 5 hours.

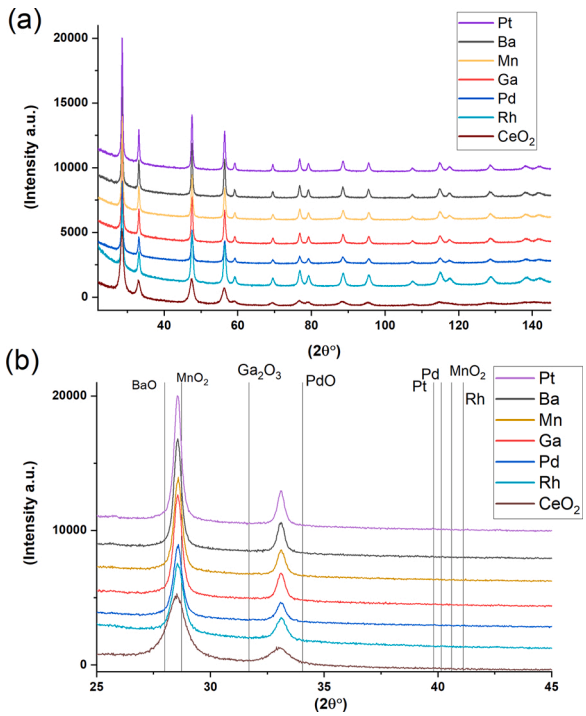

Fig. 3. (a) XRD patterns for selected surface doped samples after aging under 50 SCCM flowing air at 800 °C for 5 hours, and the as-prepared, unaged ceria powder shown for reference; (b) magnified view showing the absence of any second phase resulting from the dopant.

experimental conditions. Since STEM images are able to see the small crystallites, we would expect differences in contrast, or localized high concentrations of the dopant, indicative of phase segregation. In the supporting information, TEM and EDS data are shown for Mn and Pd which are representative of the other dopants that helped to preserve the surface area of ceria (Figure S2-S3). The STEM images do not show any contrast associated with crystalline particles of a second phase. EDS analysis performed on multiple areas of each sample in spot mode confirmed that the dopants are well dispersed, and no segregation is evident.

The STEM EDS data (Figure S2-S3) confirms the presence of the dopants. The lack of atomic number contrast between the dopant atoms and Ce (Z = 58) makes direct imaging of dopant atoms on ceria very challenging. We have shown previously that the isolated Pt atoms (Z = 79) can be readily seen via AC-STEM [11,12]. AC STEM and EDS analysis was performed on the sample that exhibited the highest BET surface area, Rh/CeO_2, as shown in Figs. 4 and 5. Despite limited atomic number contrast, Rh (Z = 45) can be imaged in favorable situations where the support shows low contrast in thin regions. Such a case is shown in Fig. 4 where a Rh atom is marked. EDS analysis of the region enclosed in the yellow box confirms the presence of Rh on the sample, but direct EDS of individual atoms is not possible since the atoms move when exposed to a focused electron beam. The mobility of surface dopant atoms makes it difficult to obtain reliable quantitative analysis of EDS from very small regions. At a lower magnification (Figure S2-S3) it is possible to perform spot analysis and obtain reasonable estimates of the average composition.

A more reliable approach to establish the dispersion of the dopant atoms is DRIFTS of adsorbed CO, which is frequently used to investigate the nature of surface metal atoms on oxide supports. The vibrational frequency of CO is sensitive to changes in coordination number and oxidation state of the metal and the nature of the bond between CO and the metal atoms (i.e. on top vs. bridged or multiply bound) [16,17]. Exposing single atoms to CO can cause them to agglomerate and also to fragment back into isolated atoms, as previously documented in the case

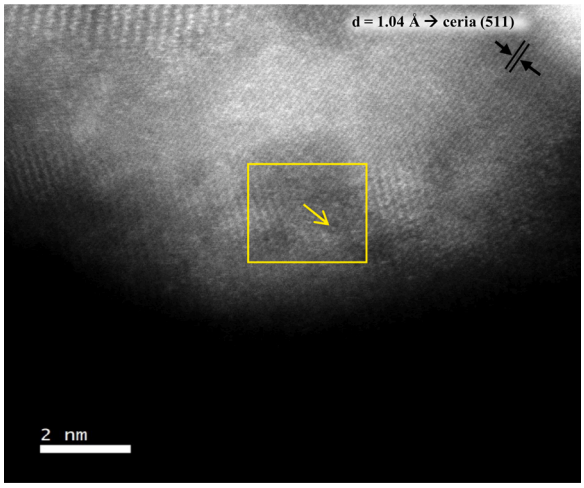

Fig. 4. HAADF AC-STEM image of Rh/ceria sample. The yellow box is the area that EDS was performed to confirm the presence of the surface dopant. The yellow arrow indicates a single atom of Rh on the surface, which is visible because of the low contrast from the support which is a result of variations in sample thickness.

of Ir [18]. Hence we performed our DRIFTS study during CO oxidation performed under lean conditions where single Pt and Pd atoms have been shown to be stable [11,19]. Fig. 6 shows the DRIFTS spectra obtained during CO oxidation for the Pt/CeO_2 and Pd/CeO_2 and Cu/CeO_2 AT samples after the gas phase CO was flushed in flowing He. We see the presence of highly symmetrical peaks, which are characteristic of CO adsorbed on single atoms [20]. Specifically, the Pt/CeO_2 sample shows a well-defined peak at 2098 cm^{-1} which has been previously assigned CO adsorbed on Pt^{2+} single atoms supported on CeO_2 [11,12,16]. Similarly, the Pd/CeO_2 sample shows a well-defined and symmetric peak at 2135 cm^{-1} which has been previously attributed to CO adsorbed on Pd^{2+} single atom species supported on CeO_2 [19]. Likewise, the Cu/CeO_2 CO band is also indicative of ionic, single atom species [21]. Moreover, no noticeable peaks are observed in any of the spectra at lower wavenumbers (< 2090 cm^{-1}) which are characteristic of CO adsorbed on metallic Pt, Pd, or Cu [19,22–24].

To verify whether the dopants were also present in the near-surface region, we performed XPS analysis of dopants that were able to stabilize surface area in excess of that provided by Pt. The XPS analysis for Pt is shown in Fig. 7 and confirms that Pt is in the +2 state. The quantification of the XPS results is shown in Table 1. It is evident that all the dopants other than Zr have a higher concentration in the near-surface region than in the bulk. While all samples were prepared with a nominal loading of 0.88 mol%, we used SEM EDS and XRF to verify the actual concentration. The XPS spectra of all the dopants is shown in Figures S6 to S12. In every instance, the dopant is in its oxidized state and the spectrum matches with that shown in the literature. The relative concentration of Ce^{3+} to total Ce detected by XPS is reported in Table 1 indicating that the $\%Ce^{3+}$ is ~ 1% and does not correlate with the dopant charge or BET surface area. This is consistent with the literature which shows that the air exposed ceria samples show very low ratios of Ce^{3+}/Ce^{4+} [25]. The peak deconvolution and quantification of the ceria peaks was performed using the method described by Kato et al [15]. The various Ce peaks are indicated in Fig. 7b. Other publications, such as Kim et al [26] and Tan et al. [27], have reported that supporting ceria on alumina helps to retain small ceria particles. The higher reported Ce^{3+} in their work could be a result of the nanosized ceria. No Zr was detected via XPS in the near-surface region. This is consistent with the known ability of Zr to form solid solutions with ceria. A recent study of ceria-zirconia confirms the depletion of Zr from the near-surface region to the bulk [28]. The lattice constant obtained from Reitveld refinement of the powder XRD shows very little variation, suggesting the dopants

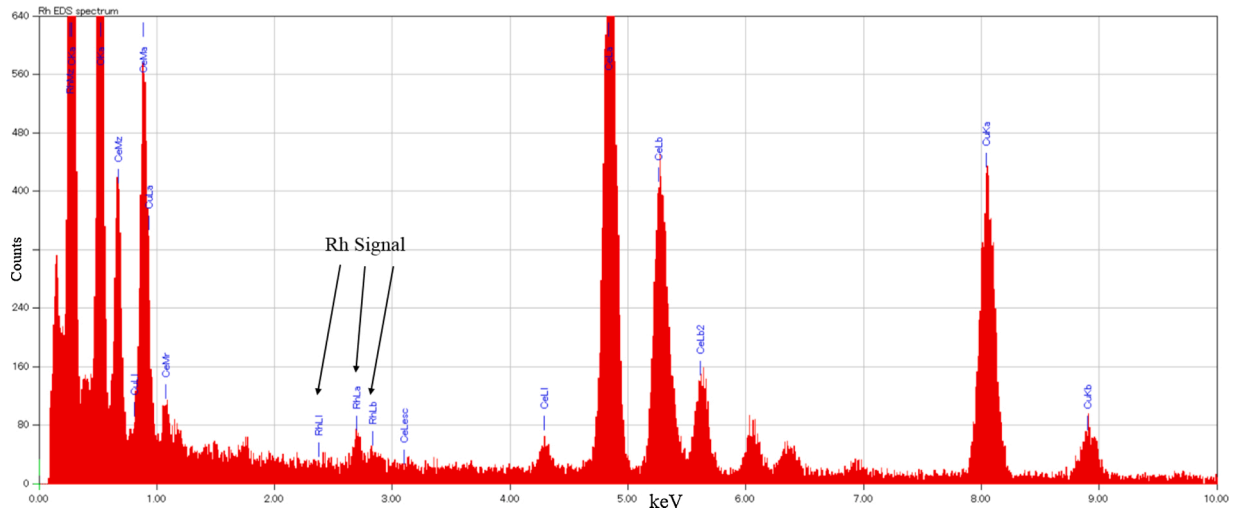

Fig. 5. EDS spectrum of the region marked with the yellow box outlined in Fig. 5 confirming the presence of Rh on the ceria.

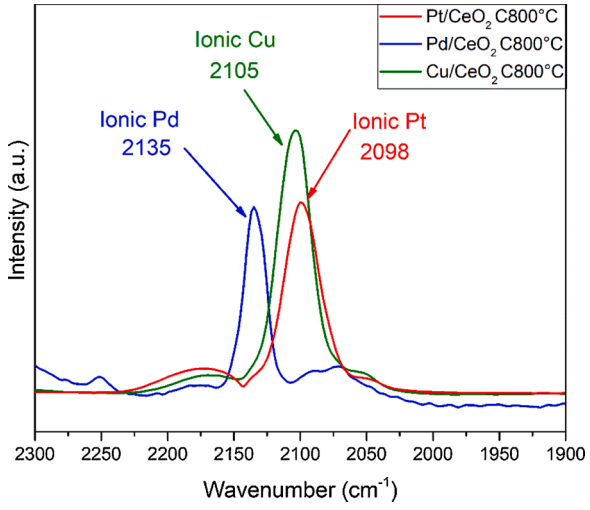

Fig. 6. CO adsorption monitored by DRIFTS during CO oxidation performed on Pt/CeO_2, Pd/CeO_2, and Cu/CeO_2 calcined at 800 °C. The spectrum was acquired after flushing with He to remove gas phase CO from the cell.

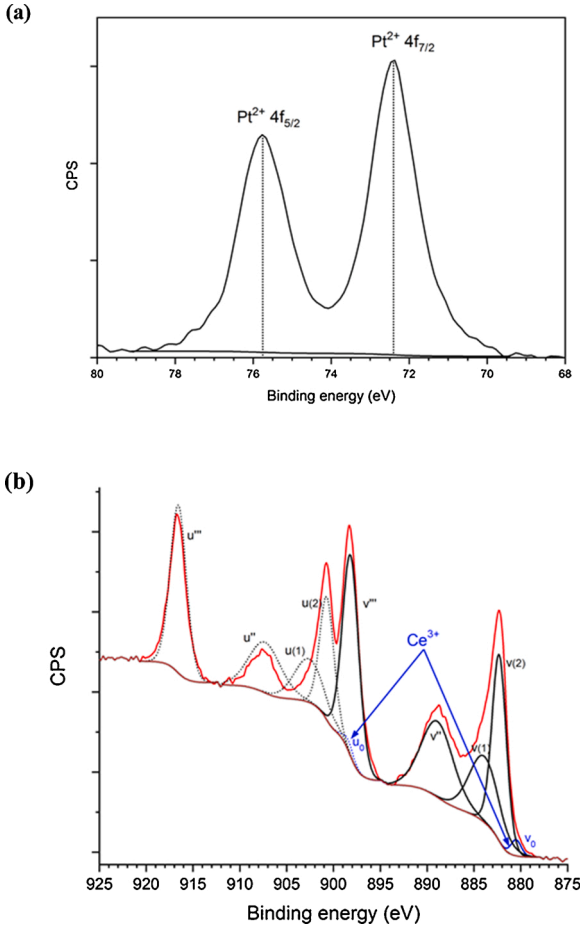

Fig. 7. (a) XPS spectra of atom trapped Pt/ceria shows the Pt is in the Pt^{2+} state. (b) XPS spectrum of Ce in this sample showing very small amount of Ce^{3+} in this air-exposed sample.

are confined to the near-surface region. The only sample that shows a slight contraction of the lattice constant is Zr, which is known to be present in the bulk (Table 1).

Since the sampling depth of XPS is several nm into the sample, we used the surface sensitive technique Low Energy Ion Scattering (LEIS) which only detects atoms at the surface. LEIS was used to determine surface concentration of the highest surface area sample, Rh/CeO_2. The signal from the powder sample was compared with a reference Rh metal foil. The Rh metal foil was first sputter cleaned, then exposed to O atoms to create an oxidized Rh surface to serve as a reference. Based on the bulk properties of Rh oxide we estimate the surface concentration of Rh in this reference sample to be ~16 atoms of Rh/nm^2 (see supporting information for more detail). When using He ions, there is not enough separation between the Rh and Ce peaks (Figure S4). However, using Ne ions (Fig. 8 and S5), there is enough separation between the peaks to allow quantitation of the Rh and Ce. Based on the peak areas, the LEIS calculation indicates that the surface concentration of Rh on the ceria surface is 0.46 atoms/nm^2. Using the BET surface area and the loading of Rh, we estimate a surface Rh concentration of 0.68 atoms/nm^2(see supporting information for more detail), which is in good agreement with the LEIS results, confirming that the Rh does not form clusters, but is atomically dispersed on the ceria surface. A similar approach [12] was used in previous work to quantify the surface concentration of Pt in samples heated in air at 800 °C, and it was concluded that the upper limit for loading was 1 atom Pt/nm^2.

Another test for the presence of dopants on the surface of ceria is measurement of catalytic reactivity. We used CO oxidation as a probe for

Table 1
Elemental analysis of ceria samples showing dopant concentration (bulk and surface), relative concentration of Ce^{3+} and XRD derived lattice constant.

Dopant Metal	Nominal Loading (mol%)	Bulk Analysis (mol%)	Surface Analysis XPS (mol%)	% Ce^{3+} by XPS (mol %)	Lattice Constant (Å)
Rh	0.88	0.93*	1.4	2.4	5.4069
Zr	0.88	1.29*	Not detected	0.8	5.4055
Pd	0.88	0.89†	3	-	5.4086
Ga	0.88	1.05†	1.3	0.9	5.4081
Al	0.88	1.26*	1.4	1.6	5.4075
Mn	0.88	0.83†	0.7	1.4	5.4080
Ba	0.88	0.64*	3.7	-	5.4098
Pt	0.88	0.93†	2.3	0.5	5.4089

* Analysis via SEM EDS
† Analysis via XRF

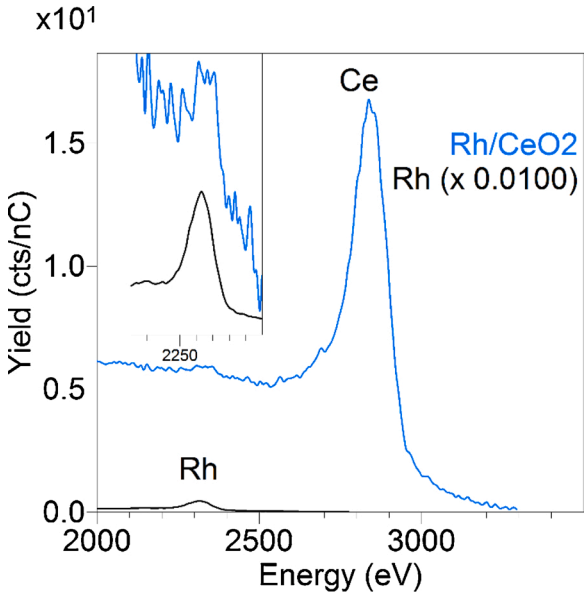

Fig. 8. The 5 keV $^{20}Ne^{+}$ spectrum for the aged Rh/ceria sample after exposure to atomic oxygen. There are peaks for Ce and Rh on the surface. The signal for the reference foil (after sputter cleaning and O atom exposure) is also shown and the inset shows the similarity of the peak shape and position confirming the presence of Rh atoms on the surface of the ceria powder.

surface dopants on the ceria focusing on those dopants that are more effective than Pt at stabilizing ceria surface area. Among these dopants, only Rh and Pd show high catalytic activity. Other dopants like Ba, Al, Mn, Ga and Zr while helping to stabilize surface area (Fig. 2) are not effective for CO oxidation (Figures S13 – S14). Hence, we report in Fig. 9 the CO oxidation reactivity of Rh and Pd along with Pt which serves as a reference. The specific reactivity, moles of CO_2 per mole of dopant per second (TOF), is reported in Fig. 10. The Pt and Pd reactivity is consistent with previous work on single atom catalysts [11,29], confirming our premise that these dopants are present at the surface. Table S2 shows that for these dopants, the reactivity does not correlate with the BET surface area. The high reactivity of Rh as a dopant suggests that it is not just the BET surface area, but the chemistry of the dopant that is responsible for the observed reactivity.

4. Discussion

The results presented here suggest that a strong interaction between the surface dopant atoms and ceria helps to keep the dopants atomically dispersed when the ceria was heated in air at 800 °C. This method of

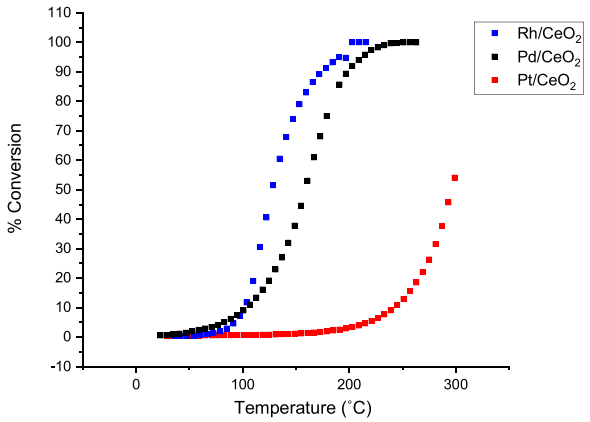

Fig. 9. CO Oxidation data for the noble metals which were all good at stabilizing ceria surface area.

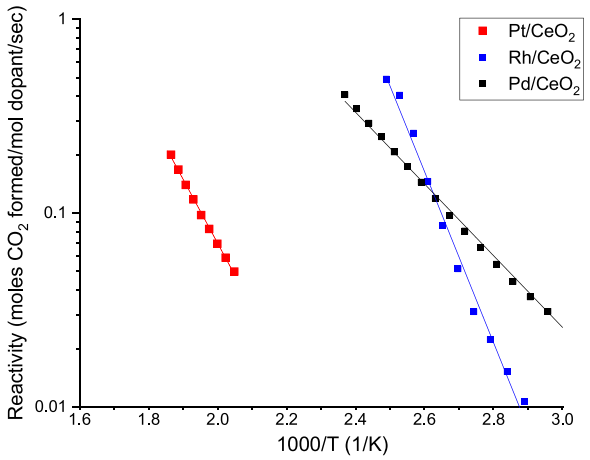

Fig. 10. Specific reactivity for CO oxidation on the noble metals, as a function of reciprocal temperature.

preparation of atomically dispersed Pt was termed 'atom trapping' [11], and it is facilitated by desorption of surface species (hydroxyls and carbonates) leaving a clean, and unsaturated, ceria surface which is able to form strong covalent bonds with the mobile surface species. TEM EDS was used to verify lack of phase segregation. Aberration corrected images of the Rh (Fig. 4) and Pt [11,12] show atomic dispersion of the dopant metal. Although it is difficult to image dopants other than Pt, due to inadequate atomic number contrast on ceria supports, under favorable conditions it is possible to detect single atoms as seen in Fig. 4. There are also no detectable second phase particles via XRD (Fig. 3 and S1). Atomic dispersion of Rh is supported by the agreement between the LEIS observed surface concentration and that calculated from the BET surface area and bulk elemental analysis. If the dopant is not atomically dispersed, the LEIS signal drops precipitously since it is sensitive only to the topmost layer of the sample [30]. The agreement between LEIS, XPS, and bulk analysis was demonstrated over a range of Pt loadings in our previous work for Pt/CeO_2 [12]. XPS analysis shows that the dopants that preserved ceria surface area better than Pt are in their ionic state and have higher concentration in the near-surface region than in the bulk. The sampling depth for XPS is 3-5 nm while LEIS is truly surface-sensitive and is sensitive only to the topmost layer. Hence the various characterization techniques indicate that the dopants are atomically dispersed on the samples heated for 5 hours in air at 800 °C.

CO oxidation was conducted on the subset of samples which showed surface area stabilization in excess of Pt. We found that the activity did not necessarily correlate with surface area, but was dependent on the

identity of the dopant. The noble metals (Pd and Rh) show high activity in CO oxidation, while Pt^{+2} bound to ceria is less active [11,12]. The high reactivity of Pd can be attributed to the high ratio of Pd^{2+} species [28]. Most of the other dopants show reactivity comparable to the undoped ceria. However, in recent work, it was shown that both Ni and Cu dopants show high reactivity in CO oxidation [31].

The Pt/ceria system is unique in that it involves vapor phase transport of Pt, in the form of PtO_2, facilitating the transport of Pt atoms to ceria. To explore whether vapor phase transport could be implicated for the other dopants, we examined the volatility of metal and oxide species likely to be present during the preparation of the doped ceria samples. Table 2 lists the available data on vapor pressure for some of the elements that were effective in preserving surface area (Figures S15-S18). Pt and Pd lie at two extremes in terms of their volatility at 800 °C in air. We have confirmed that when aging Pd/alumina catalysts in air, the thermodynamically stable phase is tetragonal PdO. As seen from Table 1, PdO is 10^7 times lower in vapor pressure than the most volatile component, PtO_2. Despite this 7 orders of magnitude difference in vapor pressure, Pd is very effective at preserving the surface area of ceria. DRIFTS was used to confirm that Pt and Pd both form atomically dispersed species after 800 °C treatment in air. The similar stabilization of ceria by Pt and Pd despite their dramatically different volatility suggests that vapor phase transport is not essential for trapping dopant atoms on the ceria surface. We, therefore, suggest that surface diffusion of the metal oxide could also be responsible for facile transport resulting in atomic dispersion of the dopant atoms [32,33]. Recent work shows that such surface diffusion is also possible on other supports such as alumina because single atom Pd species were detected after heating in air at 750 °C [34] and also previously on La-alumina [35]. It is well known that surface mobility should be expected when the temperature exceeds 50% of the bulk melting point (the Tamman temperature) [36]. Since we heated our samples to 800 °C, it is possible that oxides with melting points as high as 1872 °C might be mobile and could migrate over the oxide surface.

The conventional approach for stabilizing ceria surface area is via co-precipitation. Zirconia and alumina [40,41] have been shown to be beneficial in generating ceria that is stable at high temperatures in automotive exhaust emission catalysts. In this work, we introduced the dopant via impregnation followed by calcination at high temperatures. It is unlikely that the dopants will be incorporated into the fluorite lattice of ceria. The properties of the dopants that are effective at stabilizing ceria surface area are listed in Table 3. The oxidation state of the cerium cation in the host lattice is +4, its ionic radius is 0.97 Å, and it has a show 8-fold coordination. The size of the stable oxide cations in Table 2 range from 0.39 Å for tetrahedral Al^{3+} to 1.35 Å for (VI coordinated) BaO. It seems unlikely that all of these cations would fit in the fluorite structure of ceria. Therefore, we need to consider the coordination of the cation at the surface of ceria. Previous work has shown that the Pt is able to adopt a stable square-planar coordination by coordinating to surface oxygens at the step edges of ceria (111). In fact, DFT calculations have proposed that four-fold oxygen coordination on CeO_2 (100) micro-facets provides square pockets for binding a number of cations [14]. Once the Pt is trapped on ceria, it is no longer volatile and is not emitted to the vapor phase [42]. Since the majority of cations we investigated can adopt a stable square planar geometry like Pt, this would explain their strong binding to the ceria surface and their ability to stabilize the ceria surface area [14]. It is possible that the mechanism of surface area stabilization through surface dopants may be a more effective approach for stabilizing the surface area of metal oxides. In a recent study, Morikawa et al. [41] reported that ceria-zirconia co-precipitates retained a surface area of ~25 m^2/g after treatment at 800 °C in air for 5 hours. The results obtained here show that Zr shows a similar stabilization except with higher surface area (38 m^2/g) while only 0.88 mol% of Zr is needed as opposed to the 50 mol% (1:1 Ce:Zr) used in the work of Morikawa et al. [41].

Table 2
Thermodynamic properties of selected dopant metals or their oxides.

Species	Vapor pressure (atm) at 800 °C	Melting point (°C)	Reference
PtO_2	$1*10^{-8}$(+)	decomposes	[37,38]
RhO_2	$1*10^{-9}$	1050	[37]
Pd metal	$1*10^{-12}$	1554.8	[37,39]
Rh and Pt metal	$P < 1*10^{-15}$	1963/1768	[37,39]
PdO	$9.8*10^{-16}$	750	[37]

(+) This is the pressure of PtO_2 in equilibrium with Pt metal at 800 °C in 1 atm. of air.

Table 3
Physical/chemical properties of some of the dopants that were determined to be effective at stabilizing ceria surface area.

Transition Metal	Oxidation State	Ionic Radius (in Å)	Preferred Coordination of Cation in Stable Oxide	Reference
Ce	+4	0.97	VIII	[43]
Cu	+2	0.57	IV (square planar)	[43,44]
Pt	+4 or +2*	0.8	VI (square planar)	[43]
Al	+3*	0.39/ 0.535	IV/VI	[43]
Pd	+2*	0.64/0.86	IV (square planar)/VI	[43,44]
Rh	+4 or +3*	0.6-0.665	VI	[43]
Ba	+2*	1.35	IV	[43,45, 46]

* determined by XPS (See SI).

While the majority of the dopants we studied appear to hinder sintering, Ag had no effect on the ceria surface area, while Fe and Co appear to accelerate the sintering of ceria (Fig. 2). All of these dopants form surface complexes on ceria, based on DFT calculations, and all have binding energies for the dopant on ceria in excess of the binding energy on a metal cluster. This would imply that they should all be atomically dispersed. Some other recent work suggests Mn migrates to the surface layers of ceria particles [47]. The difference for CeO_2 stabilization among the dopants is that the binding is weakest in the case of Ag, and this might explain why the surface area is very similar to undoped ceria. While Fe and Co should be strongly bound to ceria, the literature [48,49] shows that these elements enhance the mobility of ceria and assist in grain boundary diffusion, which helps ceria sintering. It is clear that suitable surface coordination is not sufficient, since dopants like Fe and Co appear to bind strongly to ceria based on DFT computations, do not form a separate phase, but actually facilitate ceria sintering [50]. The mechanisms for ceria surface area stabilization and the relative efficacy of bulk and surface dopants needs further study in view of the commercial importance of ceria supports in heterogeneous catalysis.

5. Conclusions

In this study, we examined a number of metal dopants to assess their ability to preserve ceria surface area. Ceria was prepared by decomposition of cerium nitrate (polyhedral ceria) and aged at 800 °C in air for 5 hours. Under these conditions, the ceria surface area drops from ~85 m^2/g in its as-prepared state to 5 m^2/g after aging. When 0.88 mole % of each dopant was added before aging the sample, the surface area was maintained as high as 45 m^2/g in the order Rh > Zr > Pd > Ga ≈ Al > Mn > Ba > Pt > Pr > Cu >> La. In contrast, Ag showed no improvement while Fe and Co were detrimental, leading to loss of ceria surface area to 2 m^2/g and growth of ceria crystallite size. DFT computations suggest that all of these dopants form surface complexes, but clearly some are more effective at preserving surface area, related in part to the strength of their bonding to the surface and their ability to either slow surface diffusion on ceria or to enhance grain boundary diffusion.

AC-STEM, LEIS and DRIFTS demonstrate that these dopant atoms are located on the ceria surface and DFT computations in the literature and previous work suggests that dopants may be located on ceria step edges.

Strongly bound dopants may pin the edge atoms of CeO_2(111) which would otherwise be responsible for ceria sintering. At the high aging temperature (e.g. 800 °C in air), there is adequate mobility of the dopant atoms, either through the vapor phase or via surface diffusion, so the dopant can segregate and form a separate phase. However, we see that the dopant is found to be atomically dispersed on the ceria surface. This atomic dispersion is facilitated by the fact that surface hydroxyls and adsorbed species such as hydrocarbons or carbonates have desorbed at this temperature, allowing the dopant to form strong covalent bonds with the ceria surface. We conclude that atomically dispersed dopants allow preservation of ceria surface area. The measurement of ceria surface area in the aged samples provides a facile approach to screen transition metals that can interact strongly with the oxide surface and form stable single atom catalysts

CRediT authorship contribution statement

Ryan Alcala: Investigation, Formal analysis, Writing - original draft, Writing - review & editing. **Andrew DeLaRiva:** Investigation, Formal analysis. **Eric J. Peterson:** Investigation, Formal analysis. **Angelica Benavidez:** . **Carlos E. Garcia-Vargas:** Investigation, Formal analysis. **Dong Jiang:** Investigation, Formal analysis. **Xavier Isidro Pereira-Hernández:** Investigation, Formal analysis, Writing - original draft, Writing - review & editing. **Hidde H. Brongersma:** Methodology, Formal analysis. **Rik ter Veen:** Investigation, Formal analysis. **Jan Staněk:** Methodology. **Jeffrey T. Miller:** Conceptualization, Writing - review & editing. **Yong Wang:** Conceptualization, Writing - review & editing. **Abhaya Datye:** Conceptualization, Methodology, Writing - original draft, Writing - review & editing, Funding acquisition, Project administration.

Declaration of Competing Interest

The authors report no declarations of interest.

Acknowledgements

The work on catalyst synthesis was supported by the NSF/ERC CISTAR which is supported by the National Science Foundation under Cooperative Agreement No. EEC-1647722. Additional support for catalyst characterization was obtained from the DOE Office of Science, Catalysis Science program, grant DE-FG02-05ER15712 (X.I.P.H and Y. W) and from the DOE Office of Energy Efficiency and Renewable Energy, Vehicle Technologies Office (C.E.G. and D.J.). We would like to thank Dr. Hiroki Hashiguchi for acquiring STEM images using the JEOL Neo-ARM microscope, whose acquisition was supported by NSF grant DMR-1828731. Xavier Isidro Pereira-Hernandez and Carlos E. García-Vargas thank Fulbright Colombia and Colciencias for the funding their Ph.D. in the U.S. We also acknowledge the Czech NanoLab Research Infrastructure supported by MEYS CR (LM2018110) for the LEIS calibrations of ceria single crystals. We thank Valery Muravev from TU/Eindhoven for helpful discussions with XPS fitting of ceria peaks.

Appendix A. Supplementary data

Supplementary material related to this article can be found, in the online version, at doi:https://doi.org/10.1016/j.apcatb.2020.119722.

References

[1] T. Montini, M. Melchionna, M. Monai, P. Fornasiero, Fundamentals and Catalytic Applications of CeO_2-Based Materials, Chem. Rev. 116 (2016) 5987–6041, https://doi.org/10.1021/acs.chemrev.5b00603.
[2] M. Boaro, S. Colussi, A. Trovarelli, Ceria-Based Materials in Hydrogenation and Reforming Reactions for CO_2 Valorization, Front. Chem. 7 (2019), https://doi.org/10.3389/fchem.2019.00028.
[3] E. Mamontov, T. Egami, R. Brezny, M. Koranne, S. Tyagi, Lattice Defects and Oxygen Storage Capacity of Nanocrystalline Ceria and Ceria-Zirconia, J. Phys. Chem. B. 104 (2000) 11110–11116, https://doi.org/10.1021/jp0023011.
[4] J. Moon, Y. Cheng, L.L. Daemen, M. Li, F. Polo-Garzon, A.J. Ramirez-Cuesta, Z. Wu, Discriminating the Role of Surface Hydride and Hydroxyl for Acetylene Semihydrogenation over Ceria through In Situ Neutron and Infrared Spectroscopy, ACS Catal. 10 (2020) 5278–5287, https://doi.org/10.1021/acscatal.0c00808.
[5] C. Riley, S. Zhou, D. Kunwar, A. De La Riva, E. Peterson, R. Payne, L. Gao, S. Lin, H. Guo, A. Datye, Design of Effective Catalysts for Selective Alkyne Hydrogenation by Doping of Ceria with a Single-Atom Promotor, J. Am. Chem. Soc. 140 (2018) 12964–12973, https://doi.org/10.1021/jacs.8b07789.
[6] G. Colón, M. Pijolat, F. Valdivieso, H. Vidal, J. Kašpar, E. Finocchio, M. Daturi, F.V. M. Pijolat, J.C. Lavalley, R.T. Baker, S. Bernal, Surface and structural characterization of Ce_x $Zr_{1-x}O_2$ CEZIRENCAT mixed oxides as potential three-way catalyst promoters, J. Chem. Soc. Faraday Trans. 94 (1998) 3717–3726, https://doi.org/10.1039/A807680D.
[7] I. Atribak, A. Bueno-López, A. García García, Thermally stable ceria–zirconia catalysts for soot oxidation by O_2, Catal. Commun. 9 (2008) 250–255, https://doi.org/10.1016/j.catcom.2007.05.047.
[8] J. Wan, J. Lin, X. Guo, T. Wang, R. Zhou, Morphology effect on the structure-activity relationship of Rh/CeO_2-ZrO_2 catalysts, Chem. Eng. J. 368 (2019) 719–729, https://doi.org/10.1016/j.cej.2019.03.016.
[9] T.M. Onn, S. Zhang, L. Arroyo-Ramirez, Y. Xia, C. Wang, X. Pan, G.W. Graham, R. J. Gorte, High-surface-area ceria prepared by ALD on Al_2O_3 support, Appl. Catal. B Environ. 201 (2017) 430–437, https://doi.org/10.1016/j.apcatb.2016.08.054.
[10] X. Chen, Y. Liu, G. Niu, Z. Yang, M. Bian, A. He, High Temperature Thermal Stabilization of Alumina Modified by Lanthanum Species, Appl. Catal. -Gen. - Appl. Catal. Gen. 205 (2001) 159–172, https://doi.org/10.1016/S0926-860X(00)00575-5.
[11] J. Jones, H. Xiong, A.T. DeLaRiva, E.J. Peterson, H. Pham, S.R. Challa, G. Qi, S. Oh, M.H. Wiebenga, X.I.P. Hernández, Y. Wang, A.K. Datye, Thermally stable single-atom platinum-on-ceria catalysts via atom trapping, Science. 353 (2016) 150–154, https://doi.org/10.1126/science.aaf8800.
[12] D. Kunwar, S. Zhou, A. DeLaRiva, E.J. Peterson, H. Xiong, X.I. Pereira-Hernández, S.C. Purdy, R. ter Veen, H.H. Brongersma, J.T. Miller, H. Hashiguchi, L. Kovarik, S. Lin, H. Guo, Y. Wang, A.K. Datye, Stabilizing High Metal Loadings of Thermally Stable Platinum Single Atoms on an Industrial Catalyst Support, ACS Catal. 9 (2019) 3978–3990, https://doi.org/10.1021/acscatal.8b04885.
[13] C.-Z. Wan, J.C. Dettling, Aluminum-stabilized ceria catalyst compositions, and methods of making the same, US4714694A, 1987. https://patents.google.com/patent/US4714694A/en (accessed August 22, 2019).
[14] A. Figueroba, G. Kovács, A. Bruix, K.M. Neyman, Towards stable single-atom catalysts: strong binding of atomically dispersed transition metals on the surface of nanostructured ceria, Catal. Sci. Technol. 6 (2016) 6806–6813, https://doi.org/10.1039/C6CY00294C.
[15] S. Kato, M. Ammann, T. Huthwelker, C. Paun, M. Lampimäki, M.-T. Lee, M. Rothensteiner, J.A. van Bokhoven, Quantitative depth profiling of Ce3+ in Pt/CeO_2 by in situ high-energy XPS in a hydrogen atmosphere, Phys. Chem. Chem. Phys. 17 (2015) 5078–5083, https://doi.org/10.1039/C4CP05643D.
[16] H.A. Aleksandrov, K.M. Neyman, K.I. Hadjiivanov, G.N. Vayssilov, Can the state of platinum species be unambiguously determined by the stretching frequency of an adsorbed CO probe molecule? Phys. Chem. Chem. Phys. 18 (2016) 22108–22121, https://doi.org/10.1039/C6CP03988J.
[17] C. Lamberti, A. Zecchina, E. Groppo, S. Bordiga, Probing the surfaces of heterogeneous catalysts by in situ IR spectroscopy, Chem. Soc. Rev. 39 (2010) 4951–5001, https://doi.org/10.1039/C0CS00117A.
[18] F. Solymosi, E. Novak, A. Molnar, Infrared spectroscopic study on carbon monoxide-induced structural changes of iridium on an alumina support, J. Phys. Chem. 94 (1990) 7250–7255, https://doi.org/10.1021/j100381a054.
[19] G. Spezzati, Y. Su, J.P. Hofmann, A.D. Benavidez, A.T. DeLaRiva, J. McCabe, A. K. Datye, E.J.M. Hensen, Atomically Dispersed Pd–O Species on CeO_2(111) as Highly Active Sites for Low-Temperature CO Oxidation, ACS Catal. 7 (2017) 6887–6891, https://doi.org/10.1021/acscatal.7b02001.
[20] H.V. Thang, G. Pacchioni, L. DeRita, P. Christopher, Nature of stable single atom Pt catalysts dispersed on anatase TiO_2, J. Catal. 367 (2018) 104–114, https://doi.org/10.1016/j.jcat.2018.08.025.
[21] D. Gamarra, G. Munuera, A.B. Hungría, M. Fernández-García, J.C. Conesa, P. A. Midgley, X.Q. Wang, J.C. Hanson, J.A. Rodríguez, A. Martínez-Arias, Structure−Activity Relationship in Nanostructured Copper−Ceria-Based Preferential CO Oxidation Catalysts, J. Phys. Chem. C. 111 (2007) 11026–11038, https://doi.org/10.1021/jp072243k.
[22] H. Jeong, J. Bae, J.W. Han, H. Lee, Promoting Effects of Hydrothermal Treatment on the Activity and Durability of Pd/CeO_2 Catalysts for CO Oxidation, ACS Catal. 7 (2017) 7097–7105, https://doi.org/10.1021/acscatal.7b01810.
[23] O. Pozdnyakova, D. Teschner, A. Wootsch, J. Kröhnert, B. Steinhauer, H. Sauer, L. Toth, F.C. Jentoft, A. Knop-Gericke, Z. Paál, R. Schlögl, Preferential CO oxidation in hydrogen (PROX) on ceria-supported catalysts, part I: Oxidation state and surface species on Pt/CeO_2 under reaction conditions, J. Catal. 237 (2006) 1–16, https://doi.org/10.1016/j.jcat.2005.10.014.
[24] P. Hollins, The influence of surface defects on the infrared spectra of adsorbed species, Surf. Sci. Rep. 16 (1992) 51–94, https://doi.org/10.1016/0167-5729(92)90008-Y.
[25] E. Abi-aad, R. Bechara, J. Grimblot, A. Aboukais, Preparation and characterization of ceria under an oxidizing atmosphere. Thermal analysis, XPS, and EPR study, Chem. Mater. 5 (1993) 793–797, https://doi.org/10.1021/cm00030a013.

[26] B.-S. Kim, H. Jeong, J. Bae, P.S. Kim, C.H. Kim, H. Lee, Lean NOx trap catalysts with high low-temperature activity and hydrothermal stability, Appl. Catal. B Environ. 270 (2020) 118871, https://doi.org/10.1016/j.apcatb.2020.118871.
[27] W. Tan, H. Alsenani, S. Xie, Y. Cai, P. Xu, A. Liu, J. Ji, F. Gao, L. Dong, E. Chukwu, M. Yang, F. Liu, Tuning Single-atom Pt1−CeO2 Catalyst for Efficient CO and C3H6 Oxidation: Size Effect of Ceria on Pt Structural Evolution, ChemNanoMat. n/a (n. d.). 10.1002/cnma.202000431.
[28] Y. Ding, Q. Wu, B. Lin, Y. Guo, Y. Guo, Y. Wang, L. Wang, W. Zhan, Superior catalytic activity of a Pd catalyst in methane combustion by fine-tuning the phase of ceria-zirconia support, Appl. Catal. B Environ. 266 (2020) 118631, https://doi.org/10.1016/j.apcatb.2020.118631.
[29] D. Jiang, G. Wan, C.E. Garcia Vargas, L. Li, X.I. Pereira Hernandez, C. Wan, Y. Wan, Elucidation of the Active Sites in Single-Atom Pd_1/CeO_2 Catalysts for Low-Temperature CO Oxidation, ACS Catal. (2020), https://doi.org/10.1021/acscatal.0c02480.
[30] S. Průša, P. Procházka, P. Bábor, T. Šikola, R. ter Veen, M. Fartmann, T. Grehl, P. Brüner, D. Roth, P. Bauer, H.H. Brongersma, Highly Sensitive Detection of Surface and Intercalated Impurities in Graphene by LEIS, Langmuir 31 (2015) 9628–9635, https://doi.org/10.1021/acs.langmuir.5b01935.
[31] C. Riley, G. Canning, A. De La Riva, S. Zhou, E. Peterson, A. Boubnov, A. Hoffman, M. Tran, S.R. Bare, S. Lin, H. Guo, A. Datye, Environmentally benign synthesis of a PGM-free catalyst for low temperature CO oxidation, Appl. Catal. B Environ. 264 (2020) 118547, https://doi.org/10.1016/j.apcatb.2019.118547.
[32] Q. Wan, F. Wei, Y. Wang, F. Wang, L. Zhou, S. Lin, D. Xie, H. Guo, Single atom detachment from Cu clusters, and diffusion and trapping on CeO2(111): implications in Ostwald ripening and atomic redispersion, Nanoscale 10 (2018) 17893–17901, https://doi.org/10.1039/C8NR06232C.
[33] M. Iachella, T. Le Bahers, D. Loffreda, Diffusion Kinetics of Gold and Copper Atoms on Pristine and Reduced Rutile TiO_2 (110) Surfaces, J. Phys. Chem. C 122 (2018) 3824–3837, https://doi.org/10.1021/acs.jpcc.7b08183.
[34] E.D. Goodman, A.C. Johnston-Peck, E.M. Dietze, C.J. Wrasman, A.S. Hoffman, F. Abild-Pedersen, S.R. Bare, P.N. Plessow, M. Cargnello, Catalyst deactivation via decomposition into single atoms and the role of metal loading, Nat. Catal. 2 (2019) 748–755, https://doi.org/10.1038/s41929-019-0328-1.
[35] E.J. Peterson, A.T. DeLaRiva, S. Lin, R.S. Johnson, H. Guo, J.T. Miller, J. Hun Kwak, C.H.F. Peden, B. Kiefer, L.F. Allard, F.H. Ribeiro, A.K. Datye, Low-temperature carbon monoxide oxidation catalysed by regenerable atomically dispersed palladium on alumina, Nat. Commun. 5 (2014) 4885, https://doi.org/10.1038/ncomms5885.
[36] W.D. Kingery, Introduction to Ceramics, Wiley, 1960.
[37] W. Martienssen, H. Warlimont, Springer Handbook of Condensed Matter and Materials Data, Springer Science & Business Media, 2006.
[38] V. Voorhees, R. Adams, The use of the oxides of platinum for the catalytic reduction of organic compounds. I, J. Am. Chem. Soc. 44 (1922) 1397–1405, https://doi.org/10.1021/ja01427a021.
[39] Periodic Table – Royal Society of Chemistry, (n.d.). https://www.rsc.org/periodic-table/ (accessed October 28, 2020).
[40] C.-Z. Wan, J.C. Dettling, Aluminum-stabilized ceria catalyst compositions, and methods of making the same, US4714694A, 1987. https://patents.google.com/patent/US4714694A/en (accessed June 24, 2019).
[41] A. Morikawa, T. Suzuki, T. Kanazawa, K. Kikuta, A. Suda, H. Shinjo, A new concept in high performance ceria–zirconia oxygen storage capacity material with Al_2O_3 as a diffusion barrier, Appl. Catal. B Environ. 78 (2008) 210–221, https://doi.org/10.1016/j.apcatb.2007.09.013.
[42] D. Kunwar, C. Carrillo, H. Xiong, E. Peterson, A. DeLaRiva, A. Ghosh, G. Qi, M. Yang, M. Wiebenga, S. Oh, W. Li, A.K. Datye, Investigating anomalous growth of platinum particles during accelerated aging of diesel oxidation catalysts, Appl. Catal. B Environ. 266 (2020) 118598, https://doi.org/10.1016/j.apcatb.2020.118598.
[43] Shannon Radii, (n.d.). http://abulafia.mt.ic.ac.uk/shannon/ptable.php (accessed June 18, 2020).
[44] C.-M. Niu, P.H. Rieger, K. Dwight, A. Wold, Preparation and properties of the system $Cu_xPd_{1-x}O$ ($0 \leqq x \leqq 0.175$), J. Solid State Chem. 86 (1990) 175–179, https://doi.org/10.1016/0022-4596(90)90132-H.
[45] J.L. Jorda, T.K. Jondo, Barium oxides: equilibrium and decomposition of BaO_2, J. Alloys Compd. 327 (2001) 167–177, https://doi.org/10.1016/S0925-8388(01)01404-9.
[46] S.C. Middleburgh, K.P.D. Lagerlof, R.W. Grimes, Accommodation of Excess Oxygen in Group II Monoxides, J. Am. Ceram. Soc. 96 (2013) 308–311, https://doi.org/10.1111/j.1551-2916.2012.05452.x.
[47] H. Zhao, H. Li, Z. Pan, F. Feng, Y. Gu, J. Du, Y. Zhao, Design of CeMnCu ternary mixed oxides as soot combustion catalysts based on optimized Ce/Mn and Mn/Cu ratios in binary mixed oxides, Appl. Catal. B Environ. 268 (2020) 118422, https://doi.org/10.1016/j.apcatb.2019.118422.
[48] E. Jud, C.B. Huwiler, L.J. Gauckler, Sintering Analysis of Undoped and Cobalt Oxide Doped Ceria Solid Solutions, J. Am. Ceram. Soc. 88 (2005) 3013–3019, https://doi.org/10.1111/j.1551-2916.2005.00567.x.
[49] T.S. Zhang, J. Ma, L.B. Kong, S.H. Chan, P. Hing, J.A. Kilner, Iron oxide as an effective sintering aid and a grain boundary scavenger for ceria-based electrolytes, Solid State Ion. 167 (2004) 203–207, https://doi.org/10.1016/j.ssi.2004.01.006.
[50] J. Wang, B. Zhang, M. Shen, J. Wang, W. Wang, J. Ma, S. Liu, L. Jia, Effects of Fe-doping of ceria-based materials on their microstructural and dynamic oxygen storage and release properties, J. Sol-Gel Sci. Technol. 58 (2011) 259–268, https://doi.org/10.1007/s10971-010-2386-3.